Desalination and Water Treatment
www.deswater.com
doi: 10.5004/dwt.2020.25233

194 (2020) 333–342
August

Deterioration of shallow costal environments using synthetic aperture radar data

Mohamed Elhag*, Jarbou A. Bahrawi

Department of Hydrology and Water Resources Management, Faculty of Meteorology, Environment & Arid Land Agriculture, King Abdulaziz University, Jeddah 21589, Saudi Arabia, emails: melhag@kau.edu.sa (M. Elhag), jbahrawi@kau.edu.sa (J.A. Bahrawi)

Received 13 July 2019; Accepted 5 January 2020

ABSTRACT

Monitoring of flashflood consequences in arid environments can be realized by using either active or passive remote sensing data based mostly on the acquisition circumstances and the tackled objectives. Mapping of sediment in shorelines is a practical example where both remote sensing data can be combined to obtain robust results. The study area located on the west coast for Saudi Arabia where the shoreline of Umluj city was under investigation after a significant flash flood took place. Remote sensing images comprise of synthetic aperture radar were utilized to map the sedimentation extent with the study area process that took place after a flash flood within the designated study area. Both images were analyzed and processed using change detection techniques to quantify the sedimentation process. The late image was registered in August 2018 while the recent image was registered in March 2019 following an unusual flash flood event that occurred within the vicinity of the study area. Sediment deposits along the shoreline of the study area increased by nearly 171% and cover sea surface area closely to 4,500 km^2. Consequently, the temporal monitoring of shorelines to map the sedimentation process thematically should be nature conservation priorities specifically in fragile ecosystems.

Keywords: Mitigation; Natural Resources; Sedimentation Deposits; Sentinel-1

1. Introduction

The implementations of Remote Sensing data in monitoring of natural resources began along with conducted images from Landsat-MSS (multi scanner system) mission launched in the 1970 s. Primarily, remote sensing data sources were limited in spatial configurations and in time, where it was viewed and analyzed as passive remote sensing data type [1,2]. The uninterrupted improvement of the empirical and semi-empirical algorithms has been comprehensively testified in the last 40 years to overcome the mismanagement of the existing natural resources [3,4]. The conventional Remote Sensing data in terms of optical images weren't always successful to achieve the expected results in natural resources management due to the weather limitations signified as the atmospheric interferences [5,6].

The rule of remote sensing data in the estimation of soil erosion in addition to the assessment of sediment transport was fairly practiced after the conspicuous improvements of the empirical equations of soil lose knowns as the revised universal soil loss equation (RUSLE) and the erosion potential method (EPM). Both of those empirical equations can be only achieved if the soil physical parameters, digital elevation model (DEM) derivatives, land use, and land cover classes, as well as the organic content of the soils, were taking into consideration [7,8]. Meanwhile, neither RUSLE nor EPM is applicable to estimate sediment transport over water

* Corresponding author.

Presented at the 7th International Conference on Sustainable Solid Waste Management, 26–29 June 2019, Heraklion, Crete Island, Greece

surfaces attributable to the lack of the crucial input parameters [9,10].

Thus, the demand for unconventional methods to estimate sediment transport over water surfaces is a challenge to pursue. Radio detection and ranging images are able to overcome the limitations of implemented soil erosion algorithms disregarding the atmospheric inferences [11–13]. Lately, free access to the European Space Agency (ESA) archives conveniences the natural resources management comprehensively [14,15].

One of the most used products in radar imaging of ESA is the Sentinel-1 instrument. The sensor produces a synthetic aperture radar (SAR) images fashioned in C-band with high spatiotemporal resolutions regardless of the weather variability [14,15]. There are several applications of SAR images in natural resources management and disaster monitoring falling essentially between land and ocean natural resources management to efficiently mitigate the crisis management of natural resources [16,17].

SAR images were used to delineate sediment deposits based on the backscattering coefficient estimation in the intertidal area of the southwest Netherlands by Van Der Wal et al. [18]. Basically, surface roughness and moisture content vertical backscattering represent the synoptic feature of sediment mapping using SAR data. Seabed roughness determined as a ripple structure correlated to the sediment mud content [19,20].

Negative correlation can be significantly drawn between sediment mud content and intertidal backscattering, while a positive correlation can be drawn between the grain size of sediments and the intertidal backscattering. Therefore, moisture contents backscatter is inefficient to differentiate intertidal zones [21,22]. The estimation of mud content and the detection of surface roughness were developed using the integral equation model on SAR images [23,24]

The shorelines of the Mediterranean region are supplementary climate change susceptible specifically the rise of sea level [25,26]. Sea level rise intensity in the Mediterranean basin puts at risk the coastal habitats in the region through the destruction of natural wetlands and seawater intrusions [25,27].

The shallow shoreline and the island's system of the western side of Saudi Arabia are considered to be fragile ecosystems due to the lack of tolerance to the human activities inside the designated study area including the influences of the climate change which hasten the seawater intrusion and accordingly the loss of the shorelines [28,29]. The urban expansion because of the flourishing tourism taking place along Saudi Arabia western shoreline jeopardizes the bird migration, mangrove habitats and shallow water fishing [30]. Such development essentials to be observed and delimited to preserve these natural habitats [31].

The goals of the contemporary investigation are to map and to quantify the sedimentation movements that occurred over water surfaces after a destructive flash flood took along with the shoreline of the coastal city of Umluj. These goals will be realized by analyzing temporal passive remote sensing data conducted from the Sentinel-1 instruments that thematically map the delignated changes in the shallow shoreline of the study area. Sedimentation mapping and anomaly detection practices were implemented to the temporal SAR images to deliver consistent outcomes based on the transdisciplinary method of histogram processing, coherent image classification method.

2. Study area and research methodology

2.1. Study area description

The city of Umluj is located at the longitude of 25°37′17.30″N and the latitude of 37° 5′56.71″E on the coast of the Red Sea fallen between Alwajh city to the north and Yanbu city to the south (Fig. 1). Lately, the city has thrived and extended tourism activities, industrial and urban expansion along the city coast shoreline [32]. The city includes several islands located 60 kilometers west of the city shoreline. These islands are Mount Hassan Island, Umm Sahar Island and Fuwaideh Island. The designated study area is characterized by natural habitats diversity. The natural habitats of the city shoreline are salt marshes, lagoons, and mangrove patches. These natural habitats are nesting the juveniles of the surrounding marine ecosystem as they are imperiled in such a fragile environment [33,34]. The study area is categorized as arid environments due to its low rainfall (16 mm/y) and its imbalanced temperature that reaches 46°C in summer, sea surface temperatures range from 21°C to 29°C throughout the year. Also, the study area is highly susceptible to flash floods as it the sink of the surrounding catchments where rainfall may reach 120 mm. The northeasterly monsoon (October and November) and the southwesterly monsoon (April and May) are the most idiosyncratic phenomena that control the climatic features of the study area along with shoreline tidal action [25].

2.2. Remote sensing data

The SAR data were obtained from the Sentinel-1 sensor. Temporal data collection was assimilated in October 2018 known as the archived image and in March 2019 known as the crisis image. The SAR images implemented in the current research belong to the S1-A satellite, with the acquisition mode of Interferometric Wide (IW) and spatial resolution of 10 × 10 m (pixel spacing). The product type of the obtained images is ground range detected with dual-polarization of VV and VH. According to De Zan, and Guarnieri [35] and Berger et al. [36], Sentinel-1A delivers C-band backscattered imaging within the range from 4.0 to 8.0 GHz of the microwave part of the electromagnetic spectrum.

2.3. SAR images processing

Primarily, SAR images necessitate pre-processing procedures to ensure noise reduction and calibration to be related directly the pixel values to the radar backscatter intensities of the reflecting objects. Image pre-processing is a multitask that needs to be considered before data processing. Orbit identification is a necessary task to identify the accurate position of the sensor and its velocity which is needed for orbit state vector correction.

Image calibration is a task needed to directly relate pixel value with the corresponding backscatter intensity of the scene. Image calibration can be achieved as follows [37]:

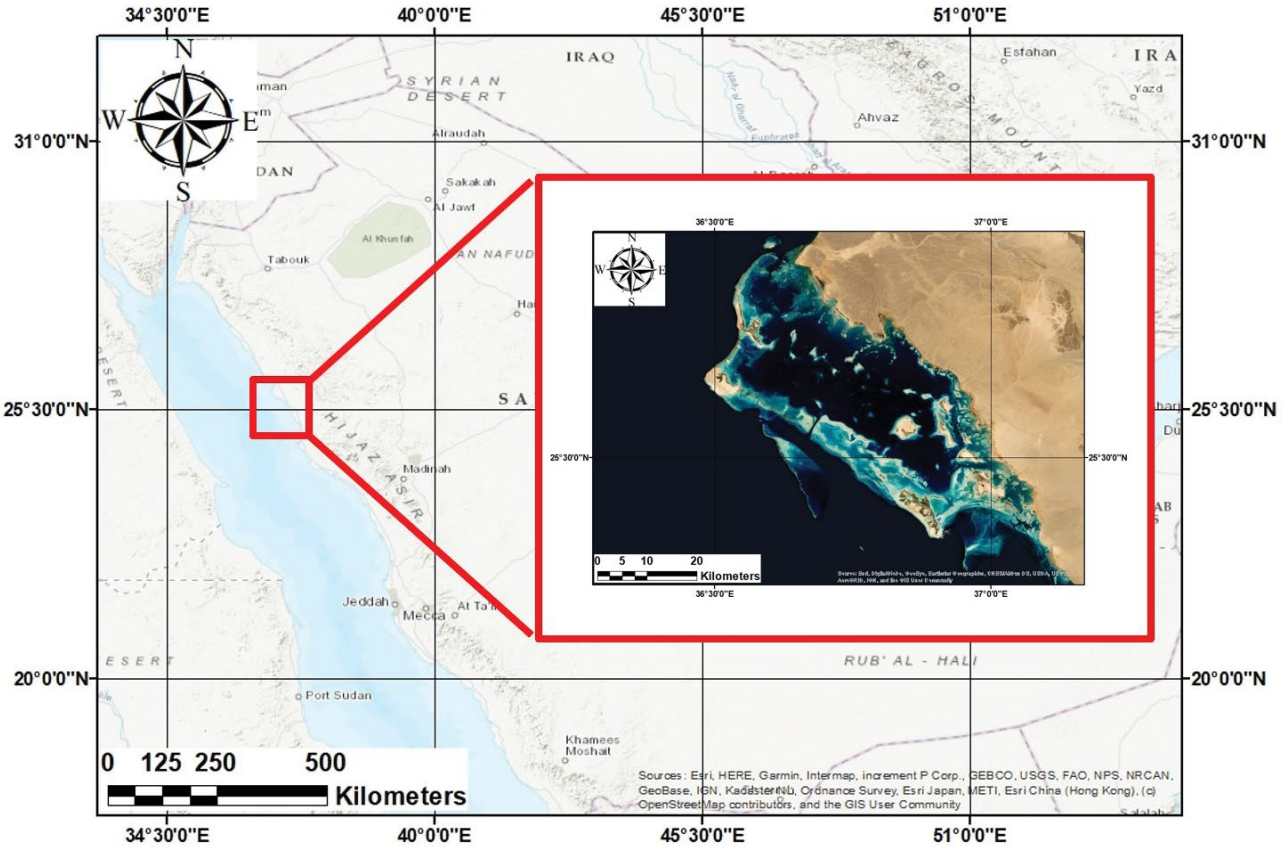

Fig. 1. Location of the study area.

$$\text{value}\left(i\right)=\frac{\left|\text{DN}_i\right|^2}{A_i^2} \tag{1}$$

where DN is the Digital Number, which one of the four LUTs that SAR level-1 data provides (DN_i, β_i, σ_i or γ_i).

Terrain correction was practiced according to Small and Schubert [38] method of orthorectification using WGS-84 as a geographic coordinate reference system. Range-Doppler correction can be realized to give earth spatial configuration (P_x, P_y, P_z) as follows:

$$f_D\left(t\right)=-\frac{2}{\gamma}.\left(\overrightarrow{v_p\left(t\right)}-\overrightarrow{v_s}\right).\left(\frac{\vec{P}-\overrightarrow{S\left(t\right)}}{\left|\vec{P}-\overrightarrow{S\left(t\right)}\right|}\right) \tag{2}$$

where $v_s(t)$ = sensor velocity at "t" time; v_p = Earth position velocity; $P = (P_x, P_y, P_z)$, at any giving location; $S_{(t)} = S_x(t)$, $S_y(t)$, $S_z(t)$, sensor position at "t" time

Consequently, the backscattered radar intensities were transformed into "sigma-nought" image according to Lee et al. [39]. Furtherly, SAR data were stacked. Consistent with Osmanoğlu et al. [40], image stacking shall be achieved as follows:

$$\gamma^m=\frac{1}{K}\sum_{K=0}^{K}g\left(B^{k,m},1,200\right)\times g\left(T^{k,m},5\right)\times g\left(f_{\text{dc}}^{k,m},1,380\right) \tag{3}$$

where B = the perpendicular baseline; m and k = the center of the image, T = the temporal baseline, f_{dc} = the Doppler baseline; c = the critical baseline.

To examine each pixel value temporally by the mean of collocating two spatially overlapping products, the coregistration task was conducted to ensure that the pixel value of the archive image is resampled into the geographical raster of the crisis image.

The adopted methodology involves temporal SAR data assessment; therefore, the image stacking is a prerequisite to conducting the assessment. In image stacking, temporal sigma-nought bands will be combined into one single image file following Osmanoğlu et al. [40] equation:

$$\gamma^m=\frac{1}{K}\sum_{K=0}^{K}g\left(B^{k,m},1,200\right)\times g\left(T^{k,m},5\right)\times g\left(f_{\text{dc}}^{k,m},1,380\right)$$

where

$$g\left(x,c\right)=\begin{cases}1-\left|x\right|/c \text{ if } \left|x\right|<c\\ 0\end{cases}, \text{otherwise} \tag{4}$$

where B = the perpendicular baseline; m and k = the center of the image, T = the temporal baseline, f_{dc} = the Doppler baseline; c = the critical baseline.

2.3. Post classification comparison

The variance in pixel values amid the early acquired image (archive image) and the lately acquired image (crisis image) can be mapped using the pixel info tool that screens the whole scene looking for the utmost variances. The foremost used techniques in anomaly detection utilizing SAR images are the ratio change and the difference change [41]. The current research adopted the difference change detection technique for easier data interpretations

$$\text{Change detection}\left(\text{Difference}\right)=\text{crises image}-\text{archive image} \tag{5}$$

2.4. Accuracy assessment

The sedimentation mapping accuracy is based on anomaly detection of SAR images of Auclair et al. [42] and Wang et al. [43]. Practically, direct ground truth accuracy assessment is not feasible because it wasn't known in advance the time of the flash flood will take place to collect corresponding samples. Therefore anomaly detection technique and its accuracy assessment come in handy to overcome ground truth sampling as simply the only anomaly feature found over water surfaces at the time of the flash flood is only the sediment[44].

The accuracy assessment was conducted to estimate omission, commission, and overall accuracy. The K_{hat} statistics is a second measure accuracy agreement. This measure of agreement is based on Congalton and Mead [45] findings. K_{hat} was calculated using the following equation:

$$K_{\text{hat}}=\frac{N\cdot\sum_{i=1}^{r}x_{ii}-\sum_{i=1}^{r}\left(x_{ij}\times x_{ji}\right)}{N^{2}-\sum_{i=1}^{r}\left(x_{ij}\times x_{ji}\right)} \tag{6}$$

where r — number of rows in the error matrix; x_{ii} — number of observations in row i and column i (the diagonal cells), x_{i+} — total observations of row i; x_{+I} — total observations of column I, N — a total of observations in the matrix.

2.5. GIS analysis

The quest of using GIS analysis is essential as the research study involves multiple data inputs that need to be stored, analyzed and produced as thematic results. The multiple layers of input data were conducted from different algorithms and exported to GIS to be probably configured. Consequently, the outcomes of the temporal SAR images processing were assigned into GIS environments for thematic interpretation of the detected shoreline changes.

SAR data were classified using an unsupervised classification algorithm due to the fact it contains only one band. Therefore the usually supervised classification algorithms won't be successful. [46]. Unsupervised classification is a deterministic decision rule [47]. Based on the calculation of the optimum index factor (OIF), the used algorithm followed Chavez [48]:

$$\text{OIF}=\frac{\sum_{k=1}s_{k}}{\sum_{j=1}\text{Abs}_{(r_{j})}} \tag{7}$$

where s_k = is the standard deviation from channel k; r_j = is the absolute value of the correlation coefficient between any of the two channels being evaluated. The schematic flowchart of the adopted methodology is illustrated in Fig. 2.

3. Results and discussion

The implemented practices on the processed SAR designed to compare the quantification of sediments using in one hand the backscattered histogram slicing to visual the range of the tackled phenomena. The sedimentation process is the key feature to be consistently assessed.

The backscattered intensities were converted into decibel (dB) sigma-nought images to be accurately envisaged [49,50].

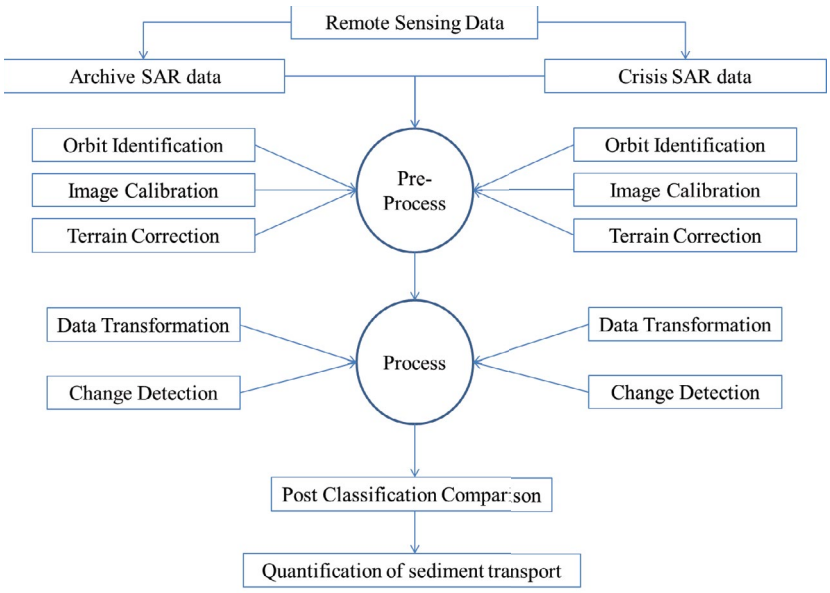

Fig. 2. Illustrates the framework methodologies adopted in the current research.

The histogram of the archive and the crisis SAR images is illustrated in Figs. 3 and 4 correspondingly. The left side of the following histograms shows the absence of data harmonization due to the numerous discrete peaks along with sigma-nought intensities of the image. Speckle filtration by means of Lee 3 × 3 windows [51] explains the targeted sigma-nought range that essentials to be measured in order to compute the sedimented pixels. The red circle displays the anomaly of backscatter intensities over water surfaces measured in dB.

Based on anomaly change detection technique over shallow water developed by Matgen et al. [52], a Boolean operator to excerpt solitary the sedimented pixels was accomplished as follows: 255*(sigma-nought crisis <–25)

The applied Boolean condition transformed the SAR images into 0 and 1 image where is 1 signifies the sedimented pixels. Assessment of the sedimented pixels was a comparatively straightforward consistent procedure since there was a notable variance to discriminate the pixels relayed on the sea surface in the archive image (Fig. 5) and the overlapped sedimented pixels obtained from the crisis image in Fig. 6 [22,50,53]. The total sedimentation area in the archive image was calculated to be 1,706 km^2 while in the crisis image the sedimentation area over of the sea surface was calculated to be 4,500 km^2.

Based on the fact that the SAR images are composed of only a single band (C-band) where most of the supervised classification algorithms will fail to classify these images [49,54]. Therefore, the use of the expectation–maximization (EM) classifier and based on OIF [55], unsupervised classification promoted five different land cover categories founded by the SAR temporal images analysis. Arithmetical and graphical analysis of the corresponded images under EM classification is shown in Figs. 7 and 8 for the archive and the crisis images respectively.

The sediment class is represented by yellow in color in Figs. 7 and 8. It is very clear that sediment movements took place after the flash flood event and dispersed over the sea surface. The quantification of the sediment movements can be accordingly estimated using a simple structured query language (SQL) method of image subtraction.

Detection of sediments according to spectral signature variabilities over water bodies is limited due to data hindering of the optical images as well as the influences of the atmospheric interaction within arid environments [56,57]. Consequently, radar images are used to improve environmental monitoring though several applications developed recently such as SAR-stacking and classification enhancements of optical/radar data fusion [58,59].

The Sentinal-1 data contributed mainly to water colorimetry classification through the sea surface measurements. The classifications were improved because of the range-Doppler terrain correction to detect sea level anomaly analysis in addition to the dynamic topography improvements of coastal environments [60–62].

Sediment movement quantification is a less complex produces to be undertaking in terrestrial ecosystems rather than aquatic ecosystems. In one hand, terrestrial ecosystems use empirical algorithms to calculate volumetrically the deposit of the sediment (ton/hectare/year) based on the utilization of the DEM derivatives to estimate the erosivity factor along with the organic content of the soils and different distribution of land use land cover classes [7,8]. On the other hand, in aquatic ecosystems, there are no topographic variables, and

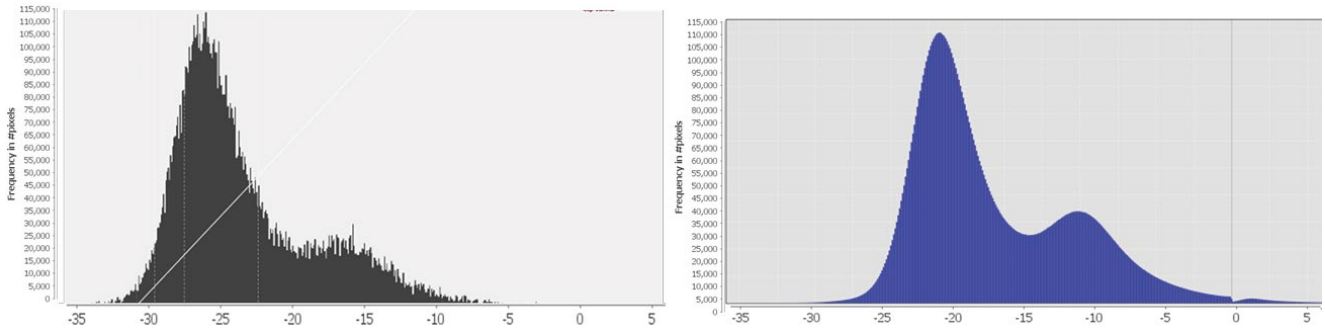

Fig. 3. Speckle filtration of the archived SAR sigma-0 intensity image in db.

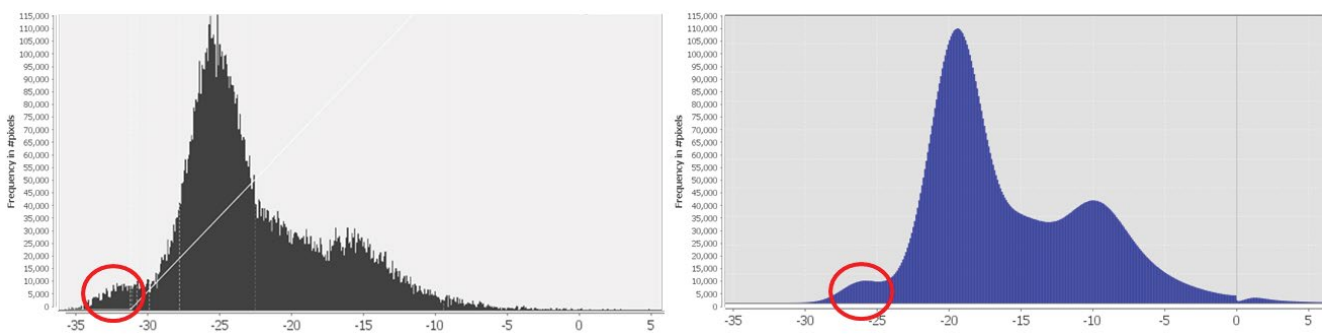

Fig. 4. Speckle filtration of the crisis SAR sigma-0 intensity image in db.

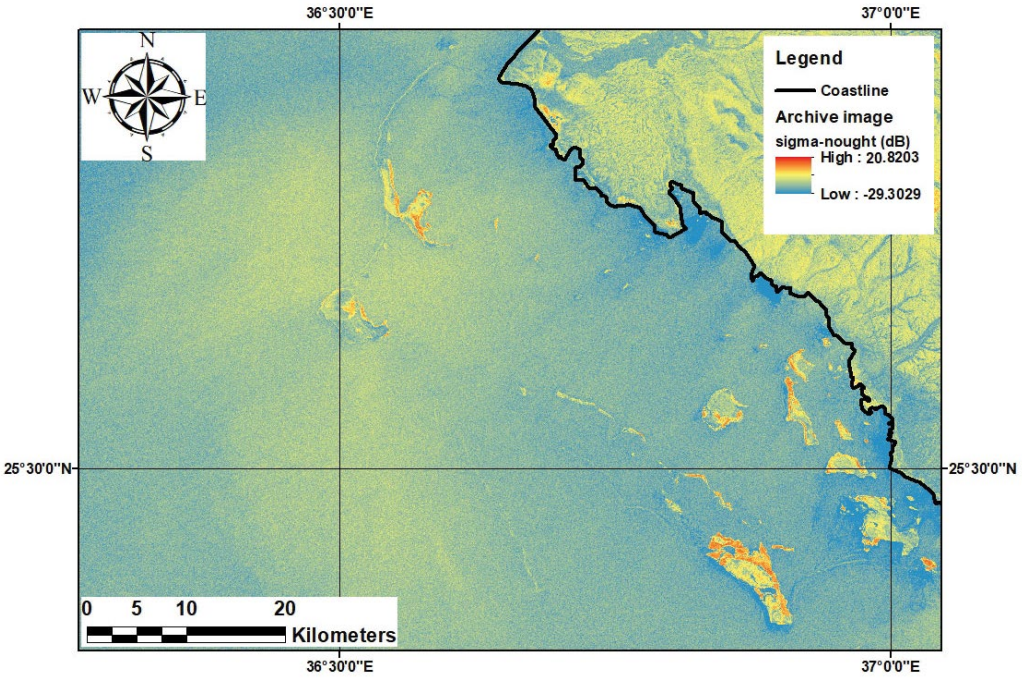

Fig. 5. Sediment deposits mapping in the SAR archive image.

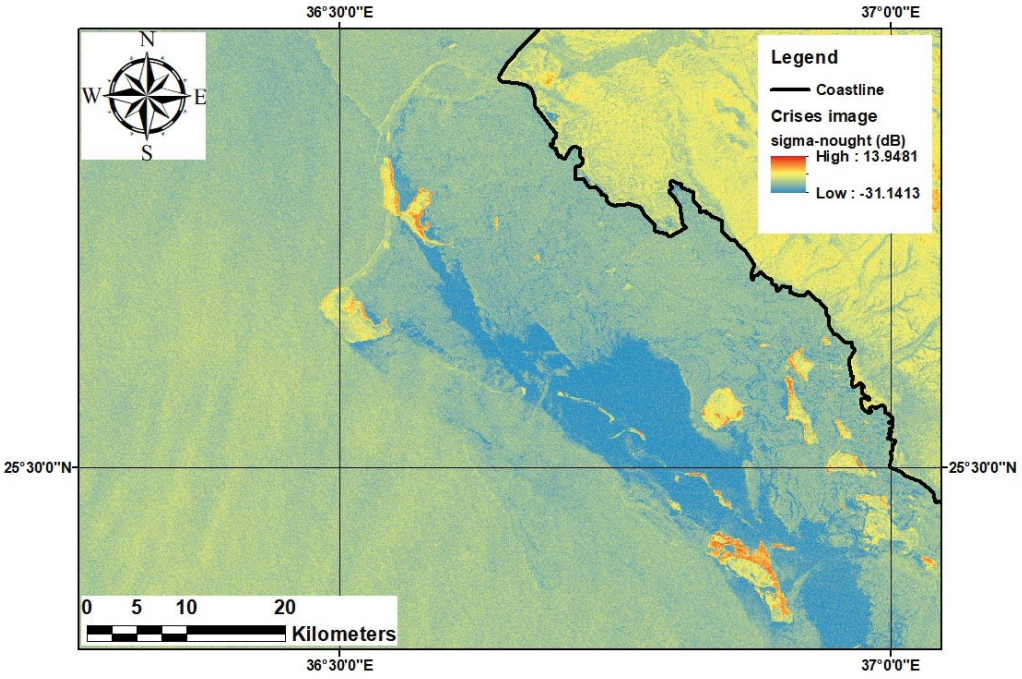

Fig. 6. Sediment deposits mapping in the SAR crisis image.

the conceivable quantification method to estimate the sedimentation progression will be comprehensibly associated with the total water surface area covered by the sediment deposits [63,64].

The rapid changes in land use land cover classes took place along with the coastal ecosystems which they are fragile and vulnerable to flash floods [7,33]. The recent flash floods that took place within the locality of the designated study area were the driving forces behind the obliteration of the natural habitats affected by the sediment movements. Conventionally, sediment deposits moved from the upper catchments and moved toward the watershed outlet into the sea can be calculated using the developed soil erosion empirical equations. Meanwhile, sediment movements

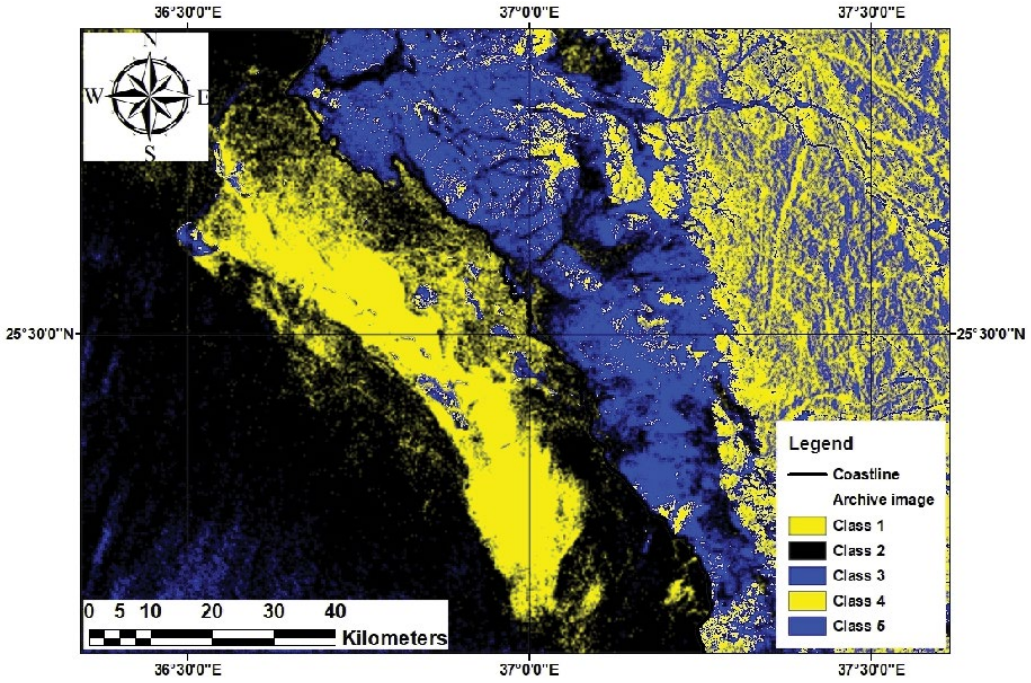

Fig. 7. Expectation-maximization classification of the early image.

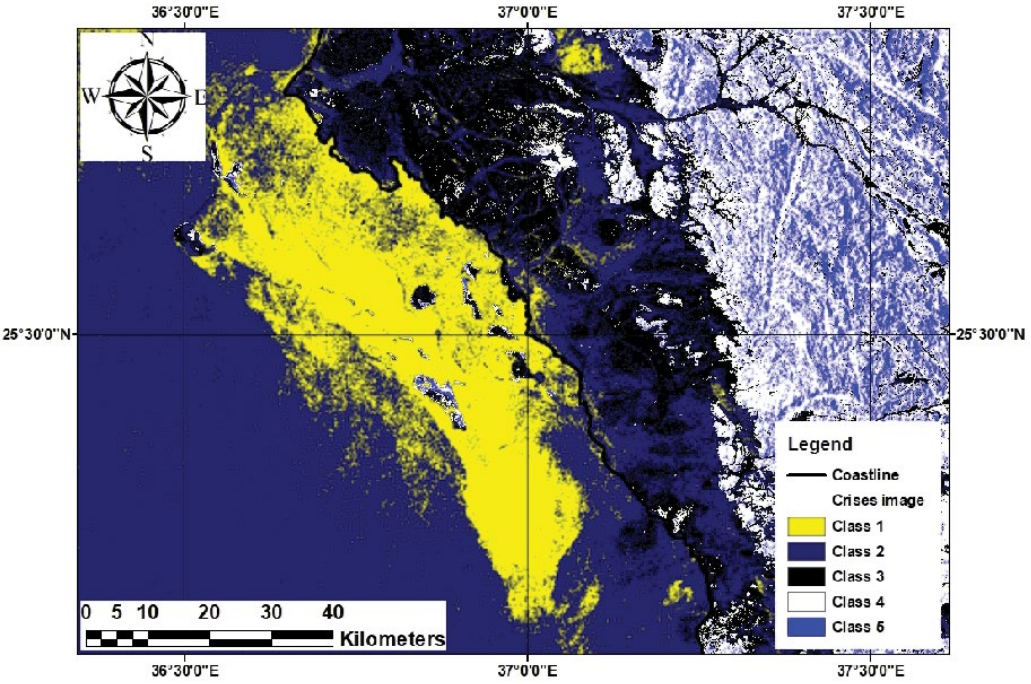

Fig. 8. Expectation-maximization classification of the late image.

over water surfaces require unconventional estimation methods that also consider tidal actions. The tidal actions and wind directions are the limiting factors of sediment dispersal over water bodies. These factors will limit the effectiveness of such a method to be time and spatial configuration-specific [65,66].

The role of climate change and its impacts on sea level rising is very essential to be considered when the sedimentation process is addressed in arid ecosystems. The sensitivity to the sea level rising of the study area as a part of Saudi Arabia western shoreline was previously discussed in several scholarly works [67]. Furthermore, human activities within

the study area accelerated the sedimentation movement along the shorelines rather than natural incidences of flash floods and tidal actions [50,68].

Biodiversity reduction along the shallow shorelines can be directly affected by the sea level rise due to the vulnerability of the coastal ecosystems [68]. Several scholarly works concerning climate change and its influence on the sea level will rise is principally assured [69,70]. Accordingly, the uncertainty range of the assumed method in the sea level rise management shall reflect the predicted mitigation scenarios of climate change [70].

Despite the fact that Saudi Arabia is located in an arid semi-arid zone, it receives distrustful flash floods from time to time because of the slender range of the mountain belt that surrounds the western shorelines of the kingdom [71]. Consistent monitoring and routine valuations of the frequent flash floods won't essentially remove the drastic effects of these events on the shallow shorelines but it will assist policymakers to reflect more consistent and more operative management plans towards the management of the shallow shorelines as well as the aquatic ecosystems [72].

4. Conclusion and Recommendations

The quantification of the sedimentation process was effectively realized in the current research using temporal SAR. SAR data were consistent in sedimentation mapping due to the penetration capabilities of the onboard C-band. The sediment deposits alongside the shoreline of the designated study area detected by SAR were counted to be 4,500 km^2 in the crisis image. Active remote sensing applications in multi-temporal data analysis provide a cost-effective and consistent approach for enhanced examination of the land use land cover change detection process. Lately, the accessibility of SAR data has overcome the limitations of optical remote sensing acquisition under unfavorable climatic conditions and makes the evaluation and the observation of the catastrophe's phenomena applicable. It is significant to inspect, in advance examination, the urban expansion within the surrounding areas due to the excess of the human activities along with climate change circumstances of sea level rising. These findings provide the standing analysis of the surrounding environments within the study area to adjust and to develop additional effectual restoration strategies. In conclusion, the outcomes of the current study robustly endorse new guidelines to take into consideration the adjacent areas that might directly or indirectly interrupt the advancement of the selected study area.

Acknowledgments

This project was funded by the Deanship of Scientific Research (DSR), King Abdulaziz University, Jeddah, under grant no. (DF-084-155-1441). The authors, therefore, acknowledge with thanks, DSR technical and financial support.

Data availability statement

The Sentinel-1 data used to support the findings of this study have been freely accessed from the ESA website "https://scihub.copernicus.eu/dhus/#/home"

References

[1] D. Tuia, M. Volpi, L. Copa, M. Kanevski, J. Munoz-Mari, A survey of active learning algorithms for supervised remote sensing image classification, IEEE J. Sel. Top. Signal Process., 5 (2011) 606–617.
[2] R.E. Kennedy, P.A. Townsend, J.E. Gross, W.B. Cohen, P. Bolstad, Y. Wang, P. Adams, Remote sensing change detection tools for natural resource managers: understanding concepts and tradeoffs in the design of landscape monitoring projects, Remote Sens. Environ., 113 (2009) 1382–1396.
[3] A.A. Mamun, A. Mahmood, M. Rahman, Identification and monitoring the change of land use pattern using remote sensing and GIS: a case study of Dhaka City, IOSR J. Mech. Civil Eng., 6 (2013) 20–28.
[4] J. Bahrawi, M. Elhag, Consideration of seasonal variations of water radiometric indices for the estimation of soil moisture content in arid environment in Saudi Arabia, Appl. Ecol. Environ. Res., 17 (2019) 285–303.
[5] G.A. Schultz, Remote sensing in hydrology, J. Hydrol., 100 (1988) 239–265.
[6] S.C. Palmer, T. Kutser, P.D. Hunter, Remote sensing of inland waters: challenges, progress and future directions, Remote Sens. Environ., 157 (2015) 1–8.
[7] J.A. Bahrawi, M. Elhag, A.Y. Aldhebiani, H.K. Galal, A.K. Hegazy, E. Alghailani, Soil erosion estimation using remote sensing techniques in Wadi Yalamlam basin, Saudi Arabia, Adv. Mater. Sci. Eng., 2016 (2016), doi: 10.1155/2016/9585962 (2016).
[8] M. Elhag, T. Kojchevska, S. Boteva, EPM for Soil Loss Estimation in Different Geomorphologic Conditions and Data Conversion by Using GIS, IOP Conference Series: Earth and Environmental Science, IOP Publishing, 221 (2019) 12079–12090.
[9] D. Yoder, G. Foster, G. Weesies, K. Renard, D. McCool, J. Lown, Evaluation of the RUSLE Soil Erosion Model, Agricultural Non-Point Source Water Quality Model: Their Use and Application, North Carolina, USA, 2001.
[10] M. Abdullah, R. Feagin, L. Musawi, The use of spatial empirical models to estimate soil erosion in arid ecosystems, Environ. Monit. Assess., 189 (2017) 78.
[11] N. Baghdadi, S. Gaultier, C. King, Retrieving surface roughness and soil moisture from synthetic aperture radar (SAR) data using neural networks, Can. J. Remote Sens., 28 (2002) 701–711.
[12] A. Vrieling, Satellite remote sensing for water erosion assessment: a review, Catena, 65 (2006) 2–18.
[13] E. Schoepfer, K. Spröhnle, O. Kranz, X. Blaes, J. Kolomaznik, F. Hilgert, T. Bartalos, T. Kemper, Towards a multi-scale approach for an Earth observation-based assessment of natural resource exploitation in conflict regions, Geocarto Int., 32 (2017) 1139–1158.
[14] M. Choi, Y. Hur, A microwave-optical/infrared disaggregation for improving spatial representation of soil moisture using AMSR-E and MODIS products, Remote Sens. Environ., 124 (2012) 259–269.
[15] A. Al-Yaari, J.-P. Wigneron, W. Dorigo, A. Colliander, T. Pellarin, S. Hahn, A. Mialon, P. Richaume, R. Fernandez-Moran, L. Fan, Assessment and inter-comparison of recently developed/reprocessed microwave satellite soil moisture products using ISMN ground-based measurements, Remote Sens. Environ., 224 (2019) 289–303.
[16] M. Horritt, D. Mason, A. Luckman, Flood boundary delineation from synthetic aperture radar imagery using a statistical active contour model, Int. J. Remote Sens., 22 (2001) 2489–2507.
[17] B. Zhang, S. Wdowinski, T. Oliver-Cabrera, R. Koirala, M. Jo, B. Osmanoglu, Mapping the extent and magnitude of sever flooding induced by hurricane Irma with multi-temporal Sentinel-1 SAR and InSAR observations, International Archives of the Photogrammetry, Remote Sens. Spatial Info. Sci., 42 (2018) 3.
[18] D. Van Der Wal, P.M. Herman, A. Wielemaker-van Den Dool, Characterisation of surface roughness and sediment texture of intertidal flats using ERS SAR imagery, Remote Sens. Environ., 98 (2005) 96–109.

[19] J.-L. Loizeau, J. Dominik, T. Luzzi, J.-P. Vernet, Sediment core correlation and mapping of sediment accumulation rates in Lake Geneva (Switzerland, France) using volume magnetic susceptibility, J. Great Lakes Res., 23 (1997) 391–402.
[20] A. Gaber, F. Soliman, M. Koch, F. El-Baz, Using full-polarimetric SAR data to characterize the surface sediments in desert areas: a case study in El-Gallaba Plain, Egypt, Remote Sens. Environ., 162 (2015) 11–28.
[21] D. Amitrano, G. Di Martino, A. Iodice, D. Riccio, G. Ruello, M.N. Papa, F. Ciervo, Y. Koussoube, High Resolution SAR for Monitoring of Reservoirs Sedimentation and Soil Erosion in Semi-Arid Regions, 2013 IEEE International Geoscience and Remote Sensing Symposium-IGARSS, IEEE, Melbourne, Australia, 2013, pp. 911–914.
[22] N. Prasad, V. Garg, P.K. Thakur, Role of SAR data in water body mapping and reservoir sedimentation assessment, ISPRS Annals of Photogrammetry, Remote Sens. Spatial Inf. Sci., 4 (2018) 151–158.
[23] K.-S. Chen, T.-D. Wu, L. Tsang, Q. Li, J. Shi, A.K. Fung, Emission of rough surfaces calculated by the integral equation method with comparison to three-dimensional moment method simulations, IEEE Trans. Geosci. Remote Sens., 41 (2003) 90–101.
[24] X. Bai, B. He, X. Li, J. Zeng, X. Wang, Z. Wang, Y. Zeng, Z. Su, First assessment of Sentinel-1A data for surface soil moisture estimations using a coupled water cloud model and advanced integral equation model over the Tibetan Plateau, Remote Sens., 9 (2017) 714.
[25] J.A. Bahrawi, M. Elhag, Simulation of sea level rise and its impacts on the Western Coastal Area of Saudi Arabia, Indian J. Geo-Mar. Sci., 45 (2016) 54–61.
[26] R. Ochoa-Hueso, S. Munzi, R. Alonso, M. Arróniz-Crespo, A. Avila, V. Bermejo, R. Bobbink, C. Branquinho, L. Concostrina-Zubiri, C. Cruz, Ecological impacts of atmospheric pollution and interactions with climate change in terrestrial ecosystems of the Mediterranean Basin: current research and future directions, Environ. Pollut., 227 (2017) 194–206.
[27] G. Gnanachandrasamy, T. Ramkumar, S. Venkatramanan, S. Chung, S. Vasudevan, Identification of saline water intrusion in part of Cauvery deltaic region, Tamil Nadu, Southern India: using GIS and VES methods, Mar. Geophys. Res., 37 (2016) 113–126.
[28] S. Fatorić, L. Chelleri, Vulnerability to the effects of climate change and adaptation: the case of the Spanish Ebro Delta, Ocean Coast, Management, 60 (2012) 1–10.
[29] K.T. Yılmaz, D. Harmancı, Y. Ünlükaplan, H. Alphan, L. Tezcan, Impacts of Agriculture on Coastal Dunes and a Proposal for Adaptation to Climate Change: the Case of the Akyatan Area in the Seyhan Delta, In: Climate Change Impacts on Basin Agro-ecosystems, Springer, Cham, Switzerland, 2019, pp. 165–182.
[30] J.L. Spaet, M.L. Berumen, Fish market surveys indicate unsustainable elasmobranch fisheries in the Saudi Arabian Red Sea, Fish. Res., 161 (2015) 356–364.
[31] J.R. Clark, Coastal Zone Management Handbook, CRC Press, New York, USA, 2018.
[32] M. Karuppasamy, M.A.B. Qurban, P.K. Krishnakumar, Oceanographic and Biological Aspects of the Red Sea, N. Rasul, I. Stewart, Eds., Oceanography, Springer, Cham, Switzerland, 2018, p. 147.
[33] M. Elhag, A.K. Hegazy, A.A. Alatar, M. Faisal, M. El-Bana, J.A. Bahrawi, A.A.M. Al-Ghamdi, Population demography and global sensitivity analysis of *Avicennia marina* on the eastern and western coasts of Saudi Arabia, Koedoe, 57 (2015), https://doi.org/10.4102/koedoe.v57i1.1317.
[34] M. Karuppasamy, M.A.B. Qurban, P.K. Krishnakumar, Metal Contamination Assessment in the Sediments of the Red Sea Coast of Saudi Arabia, Oceanographic and Biological Aspects of the Red Sea, Springer, Cham, Switzerland, 2019, pp. 147–170.
[35] F. De Zan, A.M. Guarnieri, TOPSAR: terrain observation by progressive scans, IEEE Trans. Geosci. Remote Sens., 44 (2006) 2352–2360.
[36] M. Berger, J. Moreno, J.A. Johannessen, P.F. Levelt, R.F. Hanssen, ESA's sentinel missions in support of Earth system science, Remote Sens. Environ., 120 (2012) 84–90.
[37] H. Laur, P. Bally, P. Meadows, J. Sánchez, B. Schättler, E. Lopinto, D. Esteban, ERS SAR Calibration: Derivation of the Backscattering Coefficient σ° in ESA ERS SAR PRI Products, ESA/ESRIN, ES-TN-RS-PM-HL09, 2003.
[38] D. Small, A. Schubert, Guide to ASAR Geocoding, ESA-ESRIN Technical Note RSL-ASAR-GC-AD, 2008.
[39] J.-S. Lee, J.-H. Wen, T.L. Ainsworth, K.-S. Chen, A.J. Chen, Improved sigma filter for speckle filtering of SAR imagery, IEEE Trans. Geosci. Remote Sens., 47 (2009) 202–213.
[40] B. Osmanoğlu, F. Sunar, S. Wdowinski, E. Cabral-Cano, Time series analysis of InSAR data: Methods and trends, ISPRS J. Photogramm. Remote Sens., 115 (2016) 90–102.
[41] B. Rosich, P. Meadows, Absolute Calibration of ASAR Level 1 Products; ESA/ESRIN, ENVI-CLVL-EOPG-TN-03–0010, 2004.
[42] M. Auclair, M. Lamothe, S. Huot, Measurement of anomalous fading for feldspar IRSL using SAR, Radiat. Meas., 37 (2003) 487–492.
[43] S. Wang, J. Li, B. Zhang, E. Spyrakos, A.N. Tyler, Q. Shen, F. Zhang, T. Kuster, M.K. Lehmann, Y. Wu, Trophic state assessment of global inland waters using a MODIS-derived Forel-Ule index, Remote Sens. Environ., 217 (2018) 444–460.
[44] A. Psilovikos, S. Margoni, An empirical model of sediment deposition processes in Lake Kerkini, Central Macedonia Greece, Environ. Monit. Assess., 164 (2010) 573–592.
[45] R.G. Congalton, R.A. Mead, A quantitative method to test for consistency and correctness in photointerpretation, Photogramm. Eng. Remote Sens., 49 (1983) 69–74.
[46] A.Y. Aldhebiani, M. Elhag, A.K. Hegazy, H.K. Galal, N.S. Mufareh, Consideration of NDVI thematic changes in density analysis and floristic composition of Wadi Yalamlam, Saudi Arabia, Geosci. Instrum. Methods Data Syst., 7 (2018) 297–306.
[47] P.H. Swain, S.M. Davis, Remote sensing: the quantitative approach, IEEE Trans. Pattern Anal. Mach. Intell., PAMI-3 (1981) 713–714.
[48] P.S. Chavez, Image-based atmospheric corrections-revisited and improved, Photogramm. Eng. Remote Sens., 62 (1996) 1025–1035.
[49] P. Manjusree, L.P. Kumar, C.M. Bhatt, G.S. Rao, V. Bhanumurthy, Optimization of threshold ranges for rapid flood inundation mapping by evaluating backscatter profiles of high incidence angle SAR images, Int. J. Disaster Risk Sci., 3 (2012) 113–122.
[50] M. Elhag, J.A. Bahrawi, Sedimentation mapping in shallow shoreline of arid environments using active remote sensing data, Nat. Hazards, 99 (2019) 879–894.
[51] J.-S. Lee, L. Jurkevich, P. Dewaele, P. Wambacq, A. Oosterlinck, Speckle filtering of synthetic aperture radar images: a review, Remote Sens. Rev., 8 (1994) 313–340.
[52] P. Matgen, G. Schumann, J.-B. Henry, L. Hoffmann, L. Pfister, Integration of SAR-derived river inundation areas, high-precision topographic data and a river flow model toward near real-time flood management, Int. J. Appl. Earth Obs. Geoinf., 9 (2007) 247–263.
[53] L. Billa, B. Pradhan, Semi-automated procedures for shoreline extraction using single RADARSAT-1 SAR image, Estuarine Coastal Shelf Sci., 95 (2011) 395–400.
[54] L.M. Dery, B. Nachman, F. Rubbo, A. Schwartzman, Weakly supervised classification in high energy physics, J. High Energy Phys., 2017 (2017) 145.
[55] J. Senthilnath, M. Kandukuri, A. Dokania, K. Ramesh, Application of UAV imaging platform for vegetation analysis based on spectral-spatial methods, Comp. Electron. Agric., 140 (2017) 8–24.
[56] J. Reiche, R. Lucas, A.L. Mitchell, J. Verbesselt, D.H. Hoekman, J. Haarpaintner, J.M. Kellndorfer, A. Rosenqvist, E.A. Lehmann, C.E. Woodcock, Combining satellite data for better tropical forest monitoring, Nat. Clim. Change, 6 (2016) 120.
[57] J.A.P. Pavanelli, J.R. Santos, L.S. Galvão, M. Xaud, H.A.M. Xaud, PALSAR-2/ALOS-2 and OLI/LANDSAT-8 data integration for land use and land cover mapping in northern Brazilian Amazon, Boletim de Ciências Geodésicas, 24 (2018) 250–269.
[58] J.J. Erinjery, M. Singh, R. Kent, Mapping and assessment of vegetation types in the tropical rainforests of the Western Ghats

using multispectral Sentinel-2 and SAR Sentinel-1 satellite imagery, Remote Sens. Environ., 216 (2018) 345–354.
[59] A. Whyte, K.P. Ferentinos, G.P. Petropoulos, A new synergistic approach for monitoring wetlands using Sentinels-1 and 2 data with object-based machine learning algorithms, Environ. Modell. Software, 104 (2018) 40–54.
[60] P. Gamba, F. Dell'Acqua, B.V. Dasarathy, Urban remote sensing using multiple data sets: past, present, and future, Inf. Fusion, 6 (2005) 319–326.
[61] C. Corbane, J.-F. Faure, N. Baghdadi, N. Villeneuve, M. Petit, Rapid urban mapping using SAR/optical imagery synergy, Sensors, 8 (2008) 7125–7143.
[62] J. Haas, Y. Ban, Sentinel-1A SAR and sentinel-2A MSI data fusion for urban ecosystem service mapping, Remote Sens. Appl.: Soc. Environ., 8 (2017) 41–53.
[63] M. Zribi, O. Taconet, S. Le Hégarat-Mascle, D. Vidal-Madjar, C. Emblanch, C. Loumagne, M. Normand, Backscattering behavior and simulation comparison over bare soils using SIR-C/X-SAR and ERASME 1994 data over Orgeval, Remote Sens. Environ., 59 (1997) 256–266.
[64] D. Amitrano, F. Ciervo, P. Di Bianco, G. Di Martino, A. Iodice, F. Mitidieri, D. Riccio, G. Ruello, M.N. Papa, Y. Koussoube, Monitoring Soil Erosion and Reservoir Sedimentation in Semi-arid Region through Remote Sensed SAR Data: A Case Study in Yatenga Region, Burkina Faso, Engineering Geology for Society and Territory-Volume 3, Springer, Cham, Switzerland, 2015, pp. 539–542.
[65] L. White, B. Brisco, M. Dabboor, A. Schmitt, A. Pratt, A collection of SAR methodologies for monitoring wetlands, Remote Sens., 7 (2015) 7615–7645.
[66] V. Abrol, M. Ben-Hur, F.G. Verheijen, J.J. Keizer, M.A. Martins, H. Tenaw, L. Tchehansky, E.R. Graber, Biochar effects on soil water infiltration and erosion under seal formation conditions: rainfall simulation experiment, J. Soils Sediments, 16 (2016) 2709–2719.
[67] M. Elhag, H.K. Galal, H. Alsubaie, Understanding of morphometric features for adequate water resource management in arid environments, Geosci. Instrum. Methods Data Syst., 6 (2017) 293.
[68] A.R. Carrasco, Ó. Ferreira, D. Roelvink, Coastal lagoons and rising sea level: a review, Earth Sci. Rev., 154 (2016) 356–368.
[69] M. Elhag, Inconsistencies of SEBS model output based on the model inputs: Global sensitivity contemplations, J Indian Soc. Remote, 44 (2016) 435–442.
[70] S. Brown, R.J. Nicholls, P. Goodwin, I. Haigh, D. Lincke, A. Vafeidis, J. Hinkel, Quantifying Land and People Exposed to Sea-Level Rise with No Mitigation and 1.5°C and 2.0°C Rise in Global Temperatures to Year 2300, Earth's Future, 6 (2018) 583–600.
[71] M. Abdulrazzak, A. Elfeki, A. Kamis, M. Kassab, N. Alamri, A. Chaabani, K. Noor, Flash flood risk assessment in urban arid environment: case study of Taibah and Islamic universities' campuses, Medina, Kingdom of Saudi Arabia, Geomatics, Nat. Hazards Risk, 10 (2019) 780–796.
[72] W. Li, H. El-Askary, M.A. Qurban, J. Li, K. ManiKandan, T. Piechota, Using multi-indices approach to quantify mangrove changes over the Western Arabian Gulf along Saudi Arabia coast, Ecol. Indic., 102 (2019) 734–745.